applied sciences

MDPI

Technical Note

Hydraulic Performance of Wave-Type Flow at a Sill-Controlled Stilling Basin

Yu Zhou [1], Jianhua Wu [2,*], Hai Zhao [3], Jianyong Hu [4] and Fuqing Bai [5]

[1] Key Laboratory for Technology in Rural Water Management of Zhejiang Province, Zhejiang University of Water Resources and Electric Power, Hangzhou 310018, China; zhouyu@zjweu.edu.cn
[2] College of Water Conservancy and Hydropower Engineering, Hohai University, Nanjing 210098, China
[3] Fuyang Forest and Water Conservancy Hydropower Bureau, Hangzhou 310018, China
[4] Zhejiang Institute of Water Resources and Ocean Engineering, Zhejiang University of Water Resources and Electric Power, Hangzhou 310018, China
[5] College of Water Conservancy and Environmental Engineering, Zhejiang University of Water Resources and Electric Power, Hangzhou 310018, China
* Correspondence: jhwu@hhu.edu.cn

Abstract: Downstream of the sluice gate or weir, wave-type flows inevitably occur in stilling basins with no tailwater. This paper aims to investigate the hydraulic performance of wave-type flows at a sill-controlled stilling basin through experimental research. The flow pattern, bottom pressure profiles along the stilling basin, and the air concentrations on the bottom and the sidewall were examined in five sill-controlled stilling basins by altering the sill position and the height. The results show that wave-type flow patterns contain submerged and non-submerged jumps, which are relevant to ambient pressure head and air entrainment. The bottom pressure profiles are related to larger pressure fluctuations at large unit discharges and two peak pressure values in the vicinity of the sill. The air concentrations on the bottom and the sidewall decrease with the increasing unit discharge. The flow zone in the vicinity of the sill should be focused upon concerning protection against cavitation damage because of the slight air entrainment and significant pressure fluctuations. These findings advance our understanding of wave-type flows, and their ambient pressure heads and air entrainment are useful for designing the sill-controlled stilling basin in hydraulic engineering.

Keywords: air entrainment; flow pattern; pressure head; sill-controlled stilling basin; wave-type flow

Citation: Zhou, Y.; Wu, J.; Zhao, H.; Hu, J.; Bai, F. Hydraulic Performance of Wave-Type Flow at a Sill-Controlled Stilling Basin. *Appl. Sci.* **2023**, *13*, 5053. https://doi.org/10.3390/app13085053

Academic Editors: Vasily Novozhilov and Cunlu Zhao

Received: 4 April 2023
Revised: 15 April 2023
Accepted: 17 April 2023
Published: 18 April 2023

1. Introduction

A hydraulic jump is a phenomenon that occurs by converting supercritical to subcritical flow regimens downstream of hydraulic structures. Hydraulic jumps mostly occur in stilling basins with sills or blocks after the sluice gates or weirs. For a sill-controlled stilling basin, the flow passing over the sill changes with the supercritical Froude number, and the relevant hydraulic characteristics (i.e., the hydraulic jump performance) are strongly influenced by the position and height of the sill [1–4]. In the stilling basin, hydraulic jumps can be classified successively into five types—namely A, B, minimum B, C, and wave-type flow—as the tailwater decreases, as illustrated in Figure 1 [5]. The A-jump corresponds practically to a classical jump as the sill position is at the end of the surface roller, and the sill has no effect on the jump (Figure 1a). The B-jump occurs when the tailwater depth decreases, the jump toe moves toward the sill and the deflection of the bottom stream occurs (Figure 1b). Consequently, the minimum B-jump is the formation of a second roller at the downstream of the sill and a C-jump forms when the maximum difference between the flow depth over the sill and the tailwater depth is realized (Figure 1c,d). As the tailwater is gradually reduced, eventually reaching the point of no tailwater, a wave-type flow will occur in the vicinity of the sill, and the resulting downstream flow is characterized by supercritical flow conditions. Distinct from other types of flow, wave-type flows result in

excessive standing waves and highly erosive supercritical flow downstream of the sill; thus, this type of flow should be generally avoided (Figure 1e). In the design of stilling basins or energy dissipators, it is very important to make sure that a hydraulic jump occurs for all possible tailwater depths. Thus, according to the practical engineering design of the sill-controlled stilling basin (i.e., an abrupt bottom rise), wave-type flow inevitably occurs when there is no tailwater [6,7].

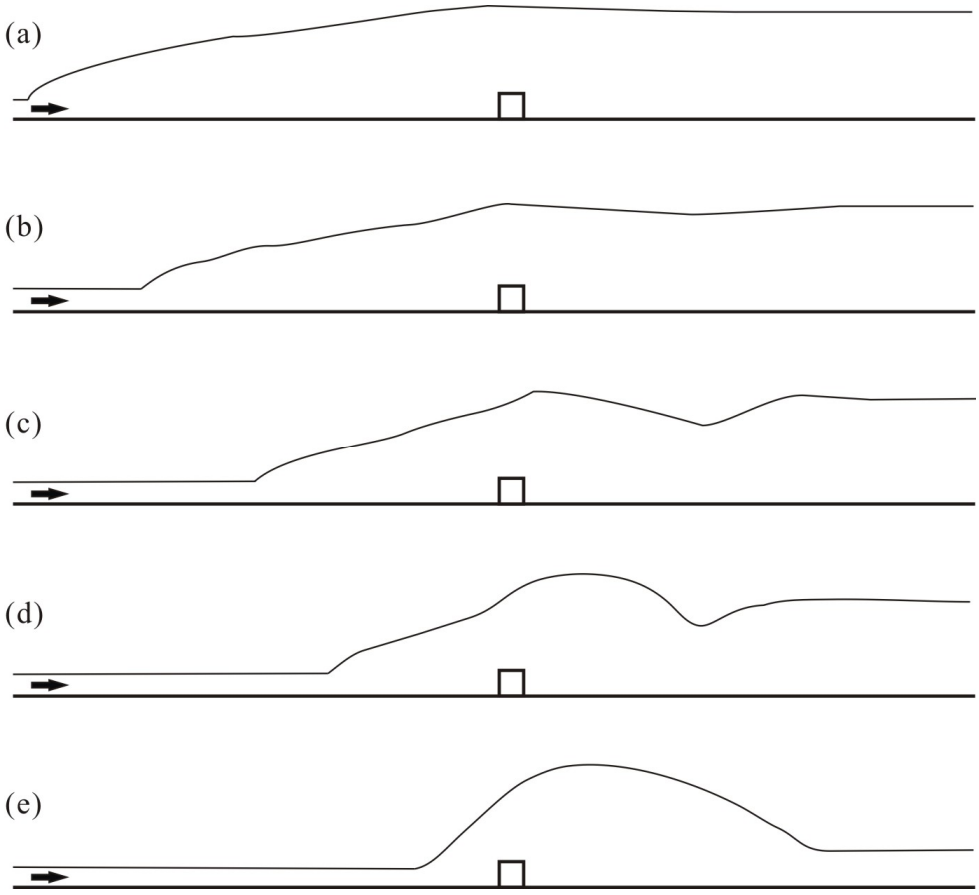

Figure 1. Sill-controlled flow: (**a**) A-jump; (**b**) B-jump; (**c**) minimum B-jump; (**d**) C-jump; (**e**) wave-type flow.

In the literature, much attention has been given to wave formation in different types of hydraulic jumps [8–10]. Different cases of wave-type flows resulting from abrupt bottom changes have been studied under supercritical downstream conditions. Kawagoshi and Hager [11] investigated the wave formation at an abrupt drop and examined various parameters, such as the sequent depth ratio, the maximum height, the location of the plunging point, the length of the downstream jump, and the resultant surface roller. Hager and Li [5] conducted an analysis on the impact of a continuous, transverse sill on the hydraulic jump in a rectangular channel. The study revealed that the jump controlled by the sill was a perturbed classical jump, as evident from the overall jump pattern. A significant reduction in the energy dissipation of the wave-type flow was observed compared to other patterns. Eroğlu and Tokyay [12] presented a simple empirical expression for determining the hydraulic characteristics of wave-type flows at abrupt bottom drops. Eroğlu and Taştan [13] analyzed the flow pattern and energy dissipation of wave-type flow when the basin bottom both rose and fell. Huang et al. [14] conducted an experimental study on wave characteristics in stilling basins with negative steps. The study describes wave height, period, probability density, and power spectrum in different stilling basins. It establishes relationships between characteristic wave heights and provides an empirical formula

for relative characteristic wave height. Zhou et al. [15] studied the energy dissipation of wave-type flow caused by a sill in the stilling basin and compared them with the data of energy dissipation by using a positive step. Moreover, a better agreement with respect to energy dissipation curves can be obtained by considering both upstream and downstream conditions.

Previous research has investigated different cases involving wave-type flows, including energy dissipation and hydraulic variables such as sequent depth ratios, maximum wave height, and wave profile. However, the effect of wave-type flows on the ambient pressure head and air entrainment has not been analyzed thoroughly. In this study, we aim to examine the hydraulic characteristics of wave-type flows, with a special focus on the bottom pressure profile along the stilling basin and the concentration of air on the bottom and sidewall. By gathering this data, it will be possible to improve the accuracy of computational fluid dynamics (CFD) models used to predict the hydraulic behavior of wave-type flows. Furthermore, the findings of this research can expand the application of sill-controlled stilling basins by developing new relationships based on the data collected.

2. Experimental Setup and Methodology

The experiments were conducted in the High-Speed Flow Laboratory at Hohai University in Nanjing, China. The experimental setup consisted of a large feeding basin, a pump, an approach conduit, a rectangular flume, a stilling basin model, and a flow return system (Figure 2). The rectangular flume made of Perspex was 25.00 m in length, 0.50 m in width, and 0.60 m in height. The stilling basin model consisted of a weir and a sill. The height of the weir P was 0.36 m. The weir was a standard Waterways Experiment Station (WES) weir with a crest profile of $y = 1.81x^{1.85}$ and a chute with an angle of 57° relative to the basin bottom. The sill in the stilling basin had a thickness and width of 0.01 m and 0.50 m. Wave-type flow was observed downstream of the weir by a sill with no tailwater conditions, and downstream flows were also supercritical.

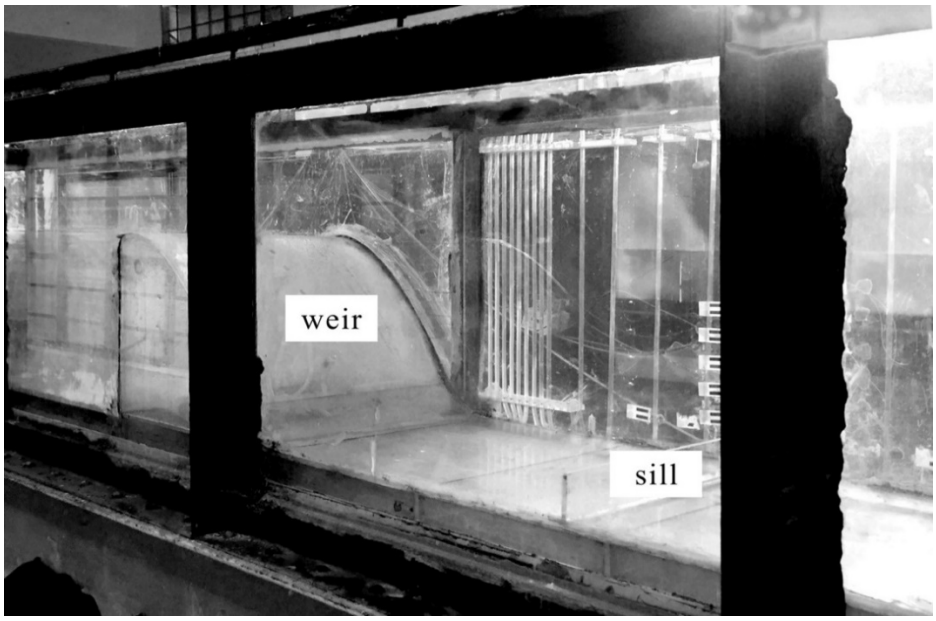

Figure 2. Experimental setup.

Figure 3 shows the experimental variables for submerged and non-submerged jumps, including the upstream flow depth, y_0; the approaching supercritical flow depth, y_1 upstream of the sill; the inflow discharge Q; the sill height, s, the length of the stilling basin, l_s (i.e., the sill position), from the weir toe (Station 0.0 m) to the upstream face of the sill; and the downstream depth, y_2. The inflow discharge, Q, was measured using a 90° V-notch weir

with an accuracy of ±1%, and flow depths y_0 and y_2 were measured using point gauges with an accuracy of ±1%. Due to the effect of free-surface instability, y_2 was measured 10 m downstream of the sill, where the free-surface undulations diminished.

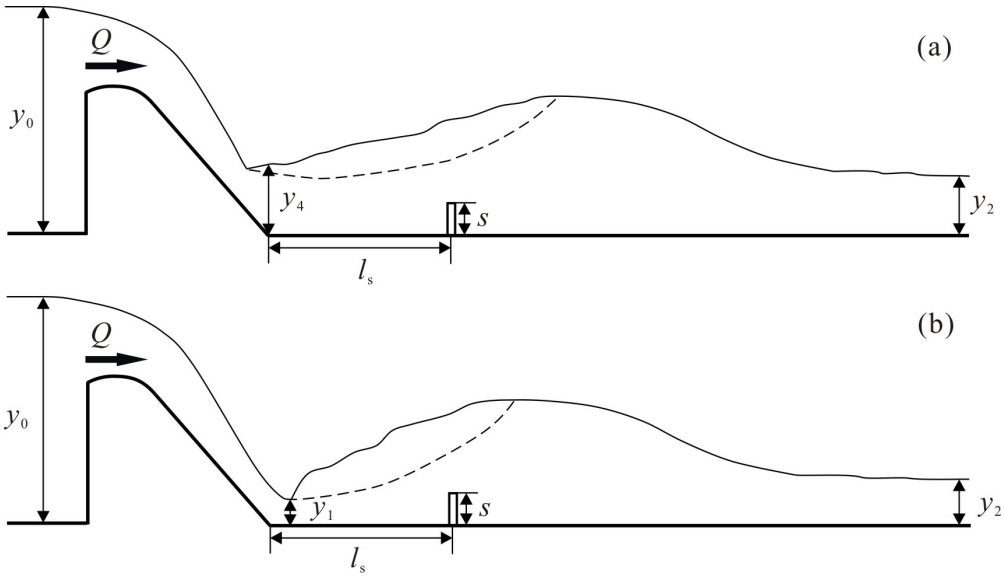

Figure 3. Experimental variables for submerged and non-submerged jumps: (**a**) submerged jump; (**b**) non-submerged jump.

Since a submerged jump may occur under certain conditions, a different method was used to calculate the flow depth y_1 and velocity v_1. For non-submerged jumps (Figure 3b), flow depth y_1 was calculated by means of an energy balance (i.e., $y_1 = E_0 - \frac{Q^2}{2gB^2\varphi^2 y_1^2}$, where E_0 is the total energy upstream of the weir, g is the acceleration of gravity, B = 0.50 m is the basin width, and φ = 0.95 is the coefficient of velocity), and velocity v_1 was calculated by means of the continuity law. For submerged jumps (Figure 3a), v_1 was calculated as $\sqrt{2g(y_0 - y_4)}$, where y_4 denotes the flow depth at the terminal section of the weir [16], and y_1 was calculated by means of the continuity law.

Figure 4 shows the layout of the air concentration and pressure measurement points. The pressure measurement points were placed at the centerline of the bottom (Figure 4b) corresponding to station 0 m, 0.05 m, 0.15 m, . . . , and 1.85 m (from the second to the last for every 0.1 m interval). The pressure on the bottom was measured with piezometric tubes with an error of ±0.5 mm. The air concentration measurement points were placed both 0.1 m off the centerline on the bottom (Figure 4b) and 0.05 m above the bottom on the sidewall at the same station (Figure 4a), which corresponds to station 0.35 m, 0.45 m, . . . , and 1.05 m (from the first to the last for every 0.1 m interval). The air concentrations both on the bottom and the sidewall were measured by using a CQ6-2005 aeration apparatus with a sampling rate of 1020 Hz, a time period of 10 s, and an error of ±0.3% [17].

For this study, the experiments were conducted for inflow unit discharges $0.102\ m^2/s \le q_w \le 0.230\ m^2/s$ (i.e., 0.102, 0.154, 0.188, 0.205 and 0.230), equaling Reynolds numbers of $3.97 \times 10^5 \le Re \le 9.14 \times 10^5$. Hence, the Reynolds numbers were large enough to avoid significant scale effects as identified in air-water flows in the stilling basin [18]. The experiments encompassed five sill-controlled stilling basins by altering the position (l_s) and height (s) of the sill. Table 1 lists the experimental flow conditions for all sill configurations comprising the upstream and downstream Froude numbers F_1 ($F_1 = v_1/\sqrt{gy_1}$) and F_2 ($F_2 = v_2/\sqrt{gy_2}$).

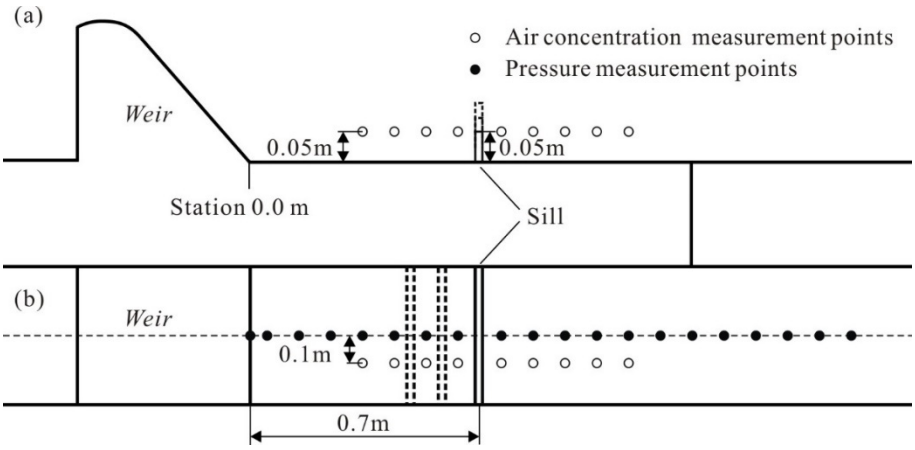

Figure 4. Layout of air concentration and pressure measurement points: (**a**) sideview; (**b**) plain view.

Table 1. Hydraulic and geometrical parameters of the sill-controlled stilling basin.

Cases	l_s (m)	s (m)	F_1	F_2	Jump Type
M12-1	0.5	0.065	5.12	1.93	SWTF
M12-2	0.5	0.065	4.21	1.65	SWTF
M12-3	0.5	0.065	3.86	1.62	SWTF
M12-4	0.5	0.065	3.77	1.72	SWTF
M12-5	0.5	0.065	3.70	1.91	SWTF
M22-1	0.6	0.065	5.18	1.66	SWTF
M22-2	0.6	0.065	4.29	1.79	SWTF
M22-3	0.6	0.065	4.13	1.87	SWTF
M22-4	0.6	0.065	3.82	1.95	SWTF
M22-5	0.6	0.065	3.74	1.77	NSWTF
M32-1	0.7	0.065	5.31	1.97	SWTF
M32-2	0.7	0.065	4.30	1.82	SWTF
M32-3	0.7	0.065	4.08	1.76	NSWTF
M32-4	0.7	0.065	3.93	2.79	NSWTF
M32-5	0.7	0.065	3.74	2.96	NSWTF
M31-1	0.7	0.050	5.26	1.44	NSWTF
M31-2	0.7	0.050	4.43	2.89	NSWTF
M31-3	0.7	0.050	4.08	3.10	NSWTF
M31-4	0.7	0.050	3.93	3.19	NSWTF
M31-5	0.7	0.050	3.74	3.13	NSWTF
M33-1	0.7	0.080	4.96	2.07	SWTF
M33-2	0.7	0.080	4.13	1.94	SWTF
M33-3	0.7	0.080	3.77	1.95	SWTF
M33-4	0.7	0.080	3.62	2.10	SWTF
M33-5	0.7	0.080	3.47	1.99	SWTF

NSWTF and SWTF are the abbreviations for non-submerged and submerged wave-type flow, respectively.

3. Results and Discussion

3.1. Flow Pattern

In most practical cases, the stilling basin with a positive step or a sill (i.e., abrupt bottom rise) was constructed to grant a forced jump inside the basin [2]. Figure 5 illustrates the wave-type flow for both Case M31 and M32 at different inflow unit discharges.

As the unit discharge increased, implying a decrease in F_1, the beginning of the jump roller moved downstream. The wave type flow exhibited a significant wave height in the vicinity of the sill, a significant water drop downstream of the sill, and the resultant downstream supercritical flow ($F_2 > 1$), as listed in Table 1. In addition, air entrainment occurred at the toe of the jump, and entrained bubbles were transported into the downstream zone.

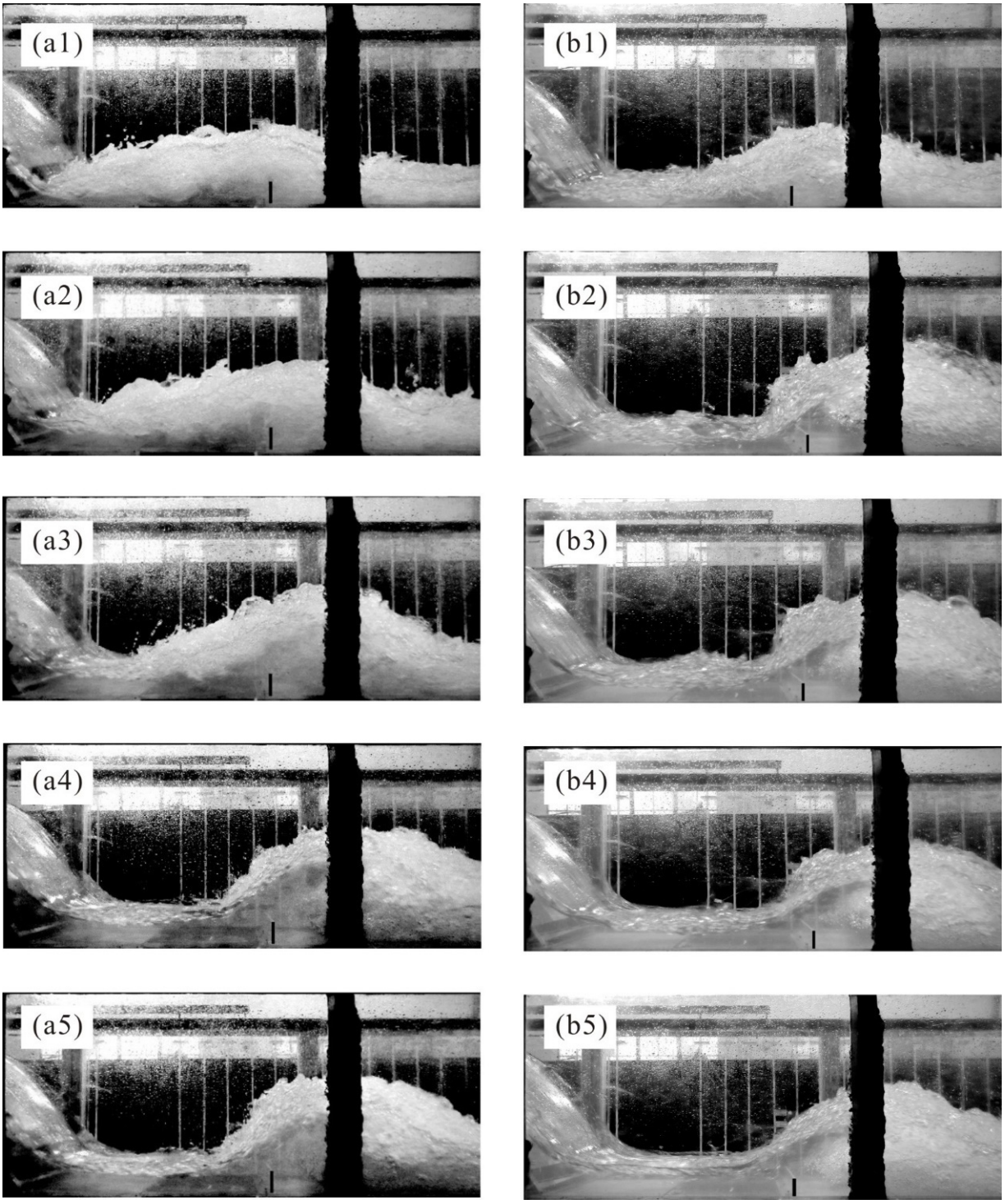

Figure 5. Wave flow pattern at different inflow unit discharges (q_w = 0.102, 0.154, 0.188, 0.205 and 0.230): (**a**) Case M31; (**b**) Case M32.

For comparison purposes, the beginning of the jump roller in Case M32 moved downstream more clearly, presenting a distinct transition from the submerged jump to the non-submerged jump, especially when the unit discharge varied from 0.154 m^2/s to 0.205 m^2/s. Moreover, the visual observations suggested a more significant amount of air in the submerged jump in Case M32, and even the entrained air could reach the stilling basin bottom.

In addition to the wave type flow, a jet flow may occur, and the curvature of the streamline approaching the sill became larger. The supercritical flow would splash over the sill and a cavity formed between the jet flow and the downstream depth [7]. Because the splash flow occurred when the relative sill height of s/y_1 was larger than its critical value, the flow pattern was closely related to inflow conditions and the sill height.

In Figure 6, the relative sill height S (i.e., $S = s/y_1$) is plotted against the upstream Froude number F_1. The data for the critical splash flow conditions are also illustrated in this figure. The relative sill height, s/y_1, in this study conformed to the wave-type flow conditions found in a previous study [7]. When wave-type flow occurred with a positive step, the flow zone behind the step could be classified into aerated or nonaerated flow. The main difference between these two wave types was that the aerated wave-type flows were associated with a better aeration effect and higher wave heights due to the subatmospheric pressure at the horizontal step surface [19].

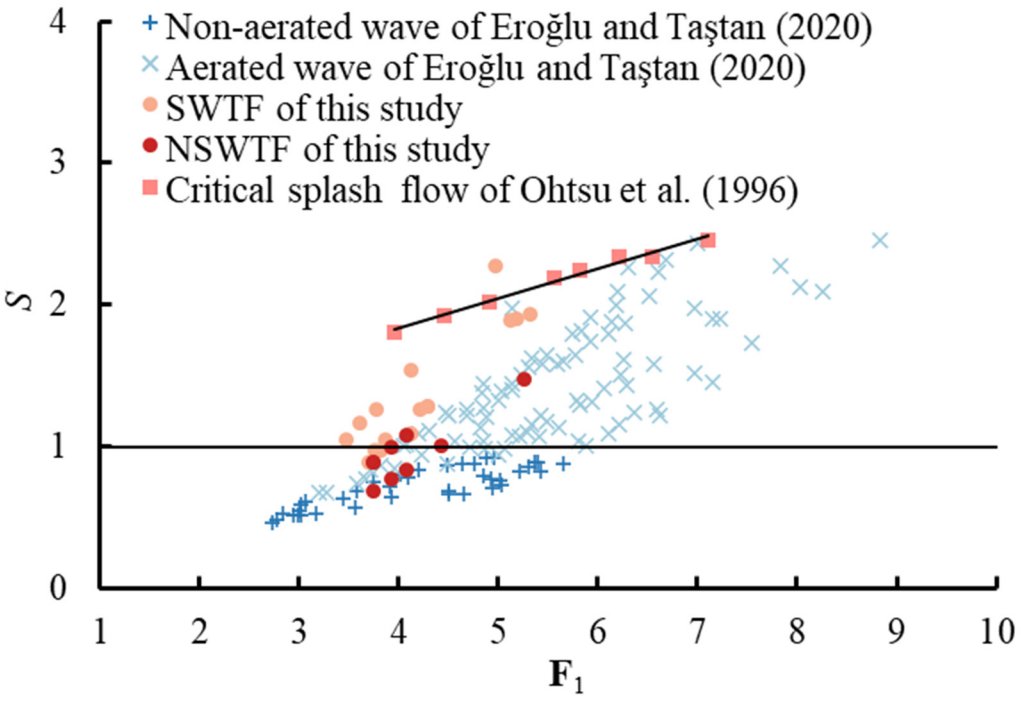

Figure 6. Relative sill height S against the upstream Froude number F_1 [7,13].

For these two wave types, the data for the relative positive step height h_s/y_1 against F_1 are also plotted in Figure 6 [13], and the line, $S = 1$, was referred to as the limit between non-wave and wave-type flows. For wave-type flow occurring with a sill in this study, the data for S against F_1 also suggest that a higher relative sill height corresponding to submerged wave-type flows is relevant for a better aeration effect, as observed in Figure 5.

3.2. Pressure Head

Figure 7 shows the maximum, mean, and minimum pressure head, H_p, on the bottom along the stilling basin starting at the weir toe (Station 0.0 m) at different unit discharges for Case M32 and a CHJ (a classical hydraulic jump). It can be observed that the bottom pressure varied greatly along the stilling basin for each unit discharge and reached a peak both at the location upstream and downstream of the sill (Figure 7a–e). Moreover, these peak values all increased with an increasing unit discharge due to the increase in water surface elevation. The maximum, mean, and minimum pressure head of a CHJ is also shown in Figure 7f, where the depth of supercritical flow (y_1) and its subcritical conjugate depth (y_2) are 0.17 m and 0.92 m, respectively, when $q_w = 0.93$ m^2/s [20]. For comparison purposes, the pressure profiles of a CHJ increased monotonically along the stilling basin,

except at its beginning. As observed in Figure 7a–e, for a small unit discharge (e.g., q_w = 0.102 m^2/s, and 0.154 m^2/s), the values of the maximum, mean, and minimum pressure were nearly the same; i.e., the pressure fluctuation along the stilling basin bottom is small. However, as the unit discharge q_w increased (q_w = 0.188 m^2/s, 0.205 m^2/s and 0.230 m^2/s, pressure fluctuations became greater in the vicinity of the sill, particularly at q_w = 0.205 m^2/s. This was attributed to the turbulent roller region of the jump, which was closer to the sill related to the transition from a submerged jump to a non-submerged jump. However, the pressure fluctuation of the classic hydraulic jump was more distinct at a near prototype scale. In order to prevent erosion below overflow spillways, chutes, and sluices, the pressure peak of wave-type flows should be carefully focused upon in this study.

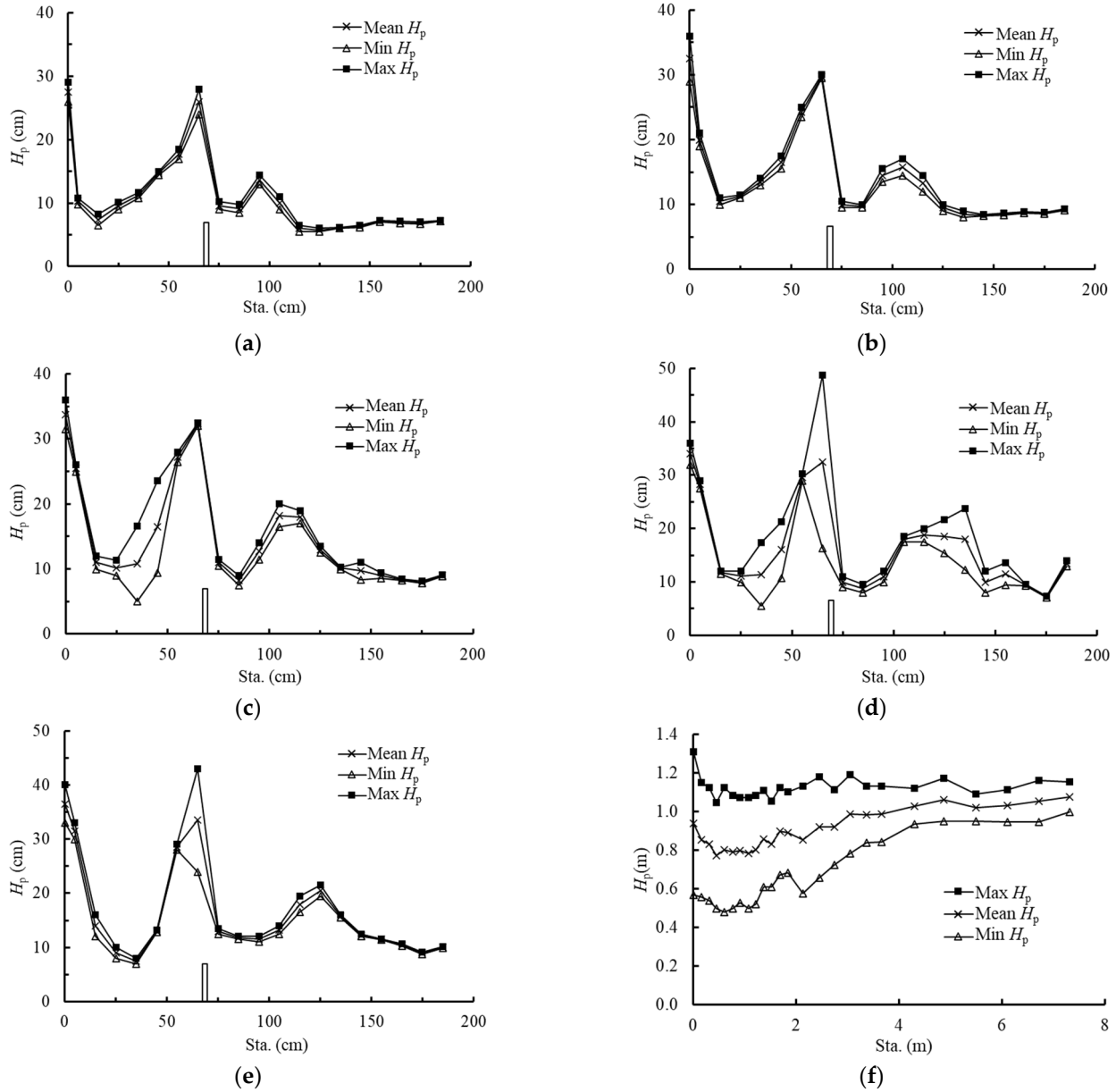

Figure 7. Maximum, mean and minimum pressure head on the bottom along the stilling basin at different unit discharges for Case M32 and a CHJ: (**a**) q_w = 0.102 m^2/s; (**b**) q_w = 0.154 m^2/s; (**c**) q_w = 0.188 m^2/s; (**d**) q_w = 0.205 m^2/s; (**e**) q_w = 0.230 m^2/s; (**f**) q_w = 0.93 m^2/s for a classical hydraulic jump [16].

Figure 8 illustrates the normalized mean pressure heads (H_p/y_2) along the stilling basin at different unit discharges (q_ws) for each case and a CHJ. In this figure, the down-

stream flow depth, y_2, was used to normalize H_p. In general, the streamwise dimensionless mean pressure heads H_p/y_2s for each case (Figure 8a–e) exhibited a similar trend at different unit discharges, with two distinct peak values observed along the stilling basin. For a CHJ in Figure 8f, H_p/y_2 typically decreased initially and then increased along the stilling basin. A larger H_p/y_2 could be obtained for a smaller q_w until the end of the jump, except for the beginning of the stilling basin. According to the existence of pressure peaks and the sill position in Figures 7 and 8, the streamwise dimensionless mean pressure indicated the following flow zones: (1) deflection zone, (2) jump zone, and (3) wave impact zone.

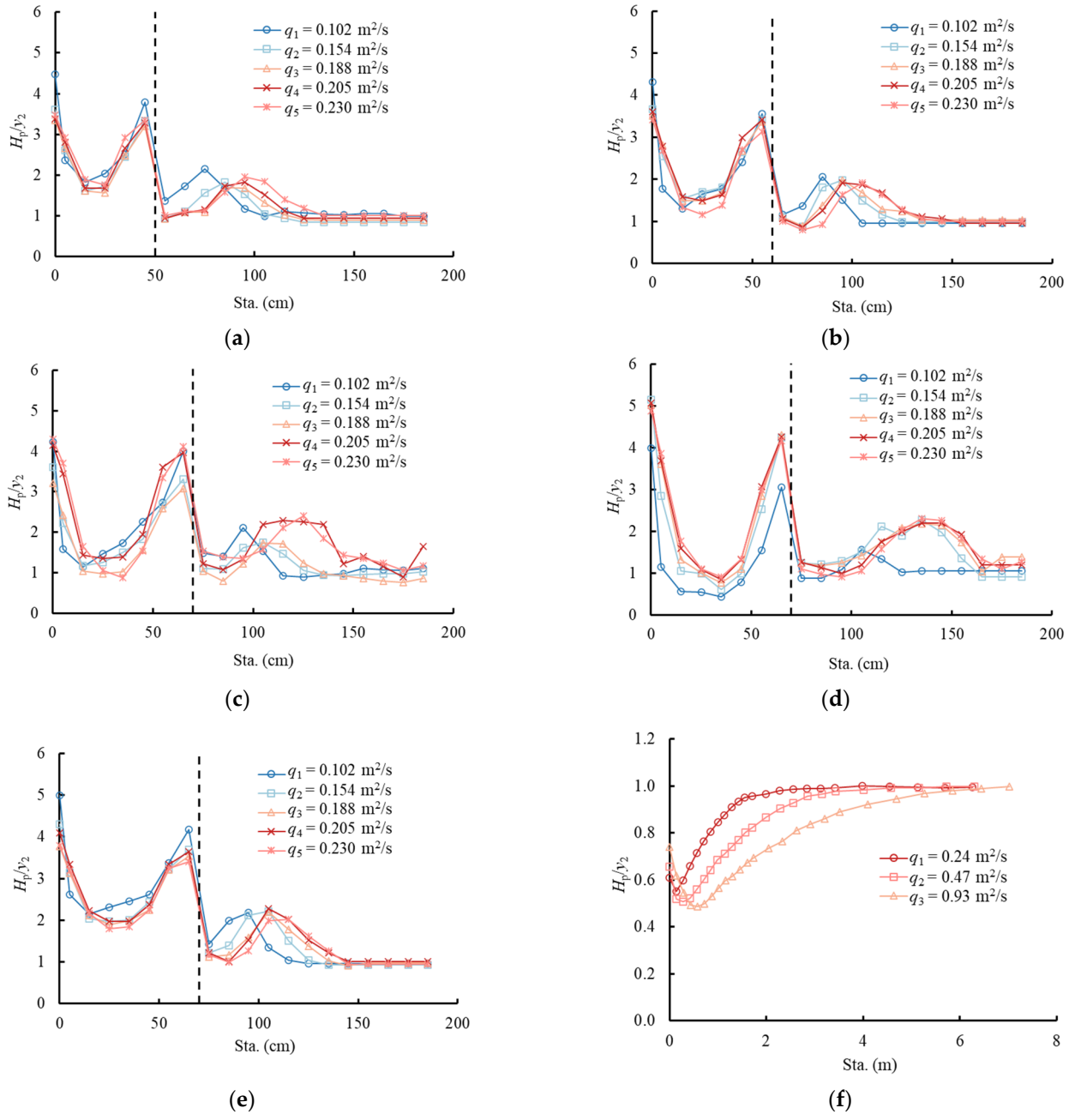

Figure 8. Normalized mean pressure head along the stilling basin for the range of q_w tested for each case: (**a**) Case M12; (**b**) Case M22; (**c**) Case M32; (**d**) Case M31; (**e**) Case M33; (**f**) Classical hydraulic jump [16].

The defection zone was characterized by the pronounced mean pressures due to the impact and curvature of the flow. In this zone, the pressure head decreased, and the

dimensional impact pressure H_p/y_2s was determined using the upstream weir flow. In the jump zone, the jump formation involved a strong pressure variation. The pressure head increased continually and reached the maximum closest to the upstream face of the sill. The resultant first peak value was much larger than the downstream depth. For the wave impact zone, wave-type flows induced a significant water drop downstream of the sill and resulted in a sudden pressure decrease and a secondary peak. The peak pressure value is still very high compared to downstream stable flow conditions y_2 (e.g., H_p/y_2 approximates 2.0 times y_2 when q_w = 0.205 m^2/s for Case M31). After the wave impact, the pressure head gradually decreased to a constant value. The pressure profile for a classical hydraulic jump by a sill—for which its position was at sta./y_2 = 5.71, 5.79, 5.87 at a unit discharge of 0.24 m^2/s, 0.46 m^2/s, and 0.93 m^2/s, respectively—is also illustrated in Figure 8f. Apart from the apparent pressure drop and wave impact in the vicinity of the sill, the mean pressure downstream of the sill was quasi-hydrostatic [21].

Generally, the designers and contractors should reinforce the stilling basin with concrete and steel to prevent the scouring of the bedrock, particularly for the local peak pressure [22]. The relative first and second peak pressure head in the vicinity of the sill normalized by the sill height H_p/s can be expressed in terms of dimensionless variables as

$$\frac{H_p}{s} = aF_1^b L^c S^d, \tag{1}$$

where $L = l_s/y_1$ and S = s/y_1 denote the relative length and height of the stilling basin, respectively; a, b, c, and d are constants. The relative first and second pressure peak values for sill configurations can be expressed with the following equations.

$$\frac{H_{p1}}{s} = 2.165F_1^{0.970} L^{0.182} S^{-0.718}, \tag{2}$$

$$\frac{H_{p2}}{s} = 3.010F_1^{0.346} L^{0.204} S^{-0.506}, \tag{3}$$

The graphs of Equations (2) and (3) are plotted in Figure 9. Equations (2) and (3) also reflected the relationships among the peak pressure heads, inflow conditions, and the sill configurations; i.e., the relative peak pressure increased with an increasing F_1 and the relative length of the stilling basin l_s/y_1 but decreased with increasing sill height s/y_1.

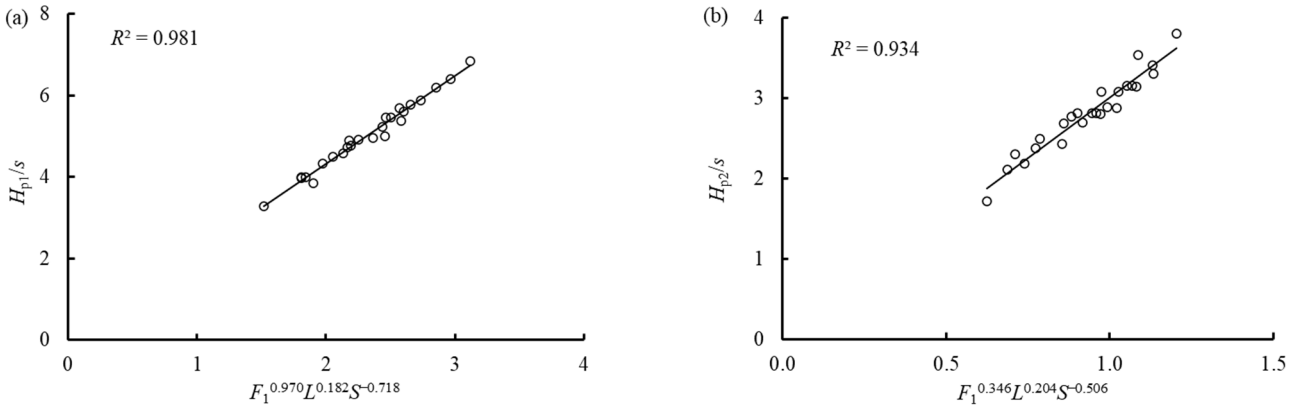

Figure 9. The relative first and second pressure peak: (**a**) first peak; (**b**) second peak.

3.3. Air Entrainment

The jump formation in the stilling basin would result in extreme water turbulence and pressure fluctuations on the bottom or the sidewall (e.g., with a restricted width) [23]. Due to the structural vibration caused by these pressure fluctuations and high velocity near the bottom of the basin, the risk of cavitation increases.

The cavitation damage can be greatly reduced by introducing enough air, and more attention should be focused upon the air concentration of the flow (i.e., the ratio of air volume to the sum of the air and water volumes) on the bottom and the sidewall. Air concentrations on the bottom (C_b) and the sidewall (C_s) in the vicinity of the sill at different inflow unit discharges q_ws for both Case M32 and M31 are highlighted in Figure 10. In this figure, $X = (x - l_s)/l_s$ represents the location of the measuring point relative to the sill position along the stilling basin floor.

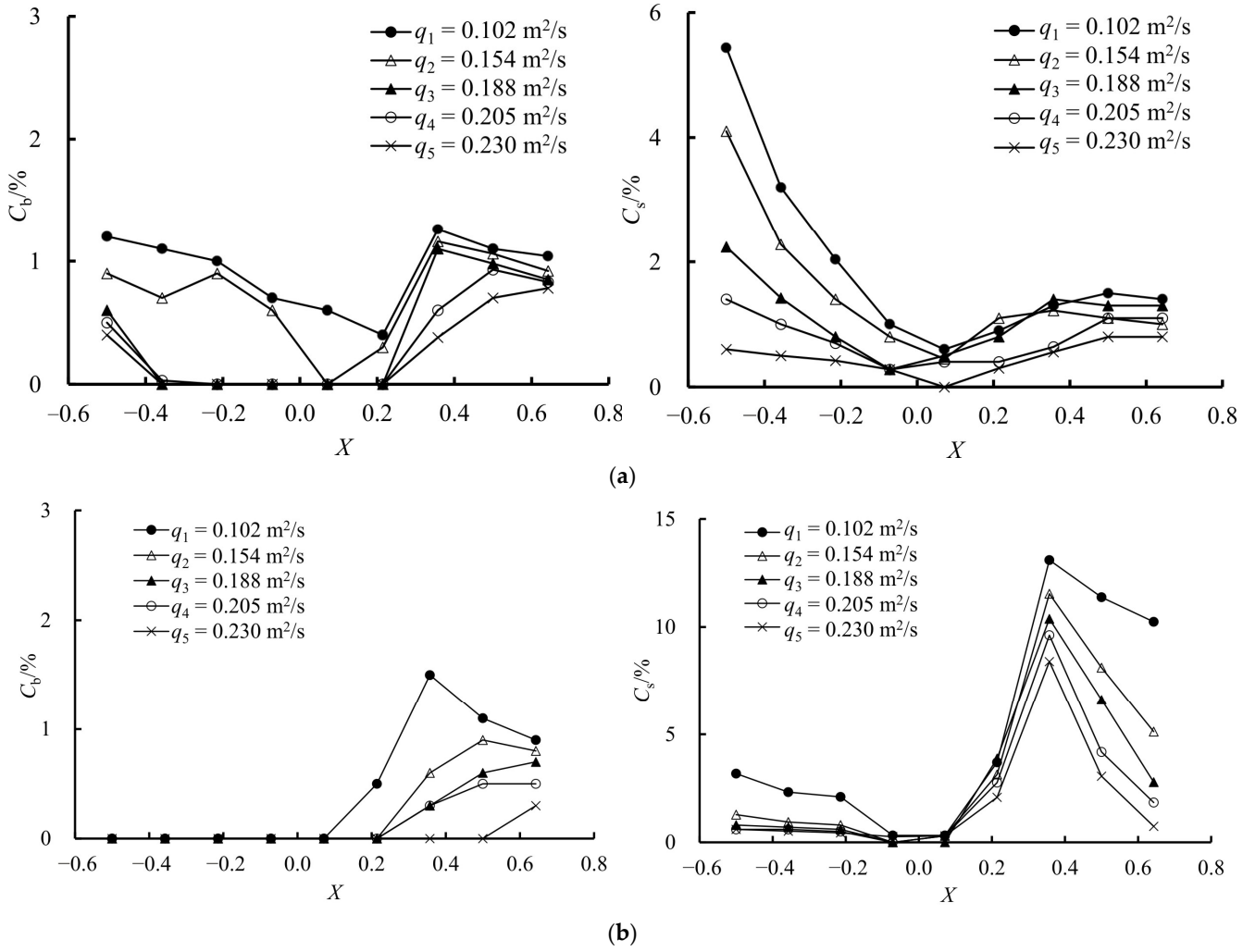

Figure 10. Air concentrations on the bottom (C_b) and the sidewall (C_s) for both Case M32 and M31 at different q_w values: (**a**) Case M32; (**b**) Case M31.

As shown in Figure 10a, air concentrations (C_b and C_s) decreased with an increasing q_w for M32. At each q_w value, a decreasing trend was observed in the upstream flow zone of the sill, and an opposite trend was found downstream of the sill. The data for M31 also exhibited the same trend at most of the flow zone in Figure 10b, but most bottom air concentrations upstream of the sill measured as zero due to the flow pattern of wave-type flows. For instance, with the increase in q_w for Case M32, the jump type changed from submerged to non-submerged, and the amount of entrained air was gradually transported downstream of the sill. At a small q_w value, entrained air resulting from the submerged jump at the toe of the weir reached the stilling basin bottom (e.g., q_w = 0.102 m^2/s and 0.154 m^2/s in Figure 5a). The blackwater zone close to the stilling basin bottom gradually enlarged with an increase in the unit discharge. In contrast, for Case M31, the flow zone upstream of the sill was always characterized by the blackwater in this study (Figure 5b).

Table 2 shows the air concentrations on the bottom and the sidewall along the stilling basin for all cases. Generally, air concentrations on the sidewall (C_s) were higher than that on the bottom (C_b). Peterka [24] proved that when the air concentration on the structure's surface was 1.0–2.0%, the cavitation damage could be considerably reduced. It was worth noting that the flow zone in the vicinity of the sill had a relatively small air concentration value (i.e., the value is below 1%) both on the bottom and the sidewall. Within these zones, the pressure profiles obviously fluctuated, especially for the location upstream of the sill, as observed in Figure 7. Thus, the resultant slight air entrainment and large pressure fluctuation should be focused upon in future work.

Table 2. Air concentrations on the bottom and the sidewall (%).

	Station (m)								
Case	**0.35**	**0.45**	**0.55**	**0.65**	**0.75**	**0.85**	**0.95**	**1.05**	**1.15**
M12-1	0.3/3.0	0/0.6	0/0	1.0/1.8	0.6/1.9	0.8/2.7	0.6/2.1	1.0/2.0	1.5/2.1
M12-2	0/1.5	0/0.3	0/0	0.7/1.0	0.5/3.4	1.1/1.1	0.7/1.5	1.0/1.8	1.8/2.2
M12-3	0/0.4	0/0	0/0	0/0.8	0.5/3.0	0.6/1.0	1.0/1.0	1.1/1.5	1.6/2.0
M12-4	0/0.3	0/0	0/0	0.3/0.8	0.6/1.1	0.8/1.0	1.3/1.4	1.4/1.6	1.5/1.8
M12-5	0/0	0/0	0/0	0/0.3	0.4/0.8	0.5/1.6	0.7/1.3	0.9/1.2	1.0/1.4
M22-1	0.6/4.4	0/2.5	0.4/1.0	0.4/0.6	1.0/1.1	0.9/0.9	1.1/2.1	0.7/8.1	0.7/1.0
M22-2	0.5/3.6	0/1.5	0.3/1.2	0/0.3	0.6/0.6	0.8/1.2	1.3/1.3	0.7/1.0	0.7/0.7
M22-3	0.4/1.5	0.3/1.7	0.3/1.0	0/0	0.4/0.4	0.9/1.2	1.0/1.0	0.7/1.1	0.7/0.7
M22-4	0/1.2	0/0.9	0/0	0/0	0/0.6	0.9/1.1	0.8/0.8	0.6/0.7	0.3/0.4
M22-5	0/1.9	0/0.4	0/0	0/0	0/0	0/1.2	0.8/1.6	0.7/1.2	0.5/0.5
M32-1	1.2/5.4	1.1/3.2	1.0/2.0	0.7/1.0	0.6/0.6	0.4/0.9	1.3/1.3	1.1/1.5	1.0/1.4
M32-2	0.9/4.1	0.7/2.3	0.9/1.4	0.6/0.8	0/0.5	0.3/1.1	1.2/1.2	1.1/1.1	0.9/1.0
M32-3	0.6/2.2	0/1.4	0/0.8	0/0.3	0/0.5	0/0.8	1.1/1.4	1.0/1.3	0.9/1.3
M32-4	0.5/1.4	0/1.0	0/0.7	0/0.3	0/0.4	0/0.4	0.6/0.6	0.9/1.1	0.8/1.1
M32-5	0.4/0.6	0/0.5	0/0.4	0/0.3	0/0	0/0.3	0.4/0.6	0.7/0.8	0.8/0.8
M31-1	0/3.2	0/2.3	0/2.1	0/0.3	0/0.3	0.5/3.7	1.5/13.1	1.1/11.4	0.9/10.2
M31-2	0/1.3	0/0.9	0/0.8	0/0	0/0.3	0/3.1	0.6/11.5	0.9/8.1	0.8/5.1
M31-3	0/0.8	0/0.7	0/0.6	0/0	0/0	0/3.9	0.3/10.4	0.6/6.6	0.7/2.8
M31-4	0/0.6	0/0.6	0/0.5	0/0	0/0.3	0/2.8	0.3/9.6	0.5/4.2	0.5/1.8
M31-5	0/0.6	0/0.5	0/0.4	0/0.3	0/0.3	0/2.1	0/8.4	0/3.1	0.3/0.7
M33-1	0.8/2.9	0.8/2.2	0.7/1.9	0.3/0.6	0.6/0.7	1.2/2.1	1.6/2.2	1.7/1.9	1.3/1.6
M33-2	0.7/2.4	0.8/1.9	0.6/1.7	0/0	0.5/0.6	1.0/1.9	1.6/2	1.6/1.7	1.2/1.4
M33-3	0.6/1.9	0.6/1.6	0.5/1.4	0/0.3	0.4/0.5	0.8/1.6	1.4/1.7	1.4/1.5	1.1/1.2
M33-4	0.6/1.3	0.6/1.2	0.5/1.3	0/0.3	0.3/0.5	0.7/1.3	1.2/1.5	1.3/1.4	1.0/1.2
M33-5	0.6/1.2	0.6/1.0	0.5/1.1	0/0	0.3/0.4	0.7/1.2	1.2/1.3	1.2/1.2	1.0/1.1

In the term "x/y" of the air concentration data, x and y are experimental data on the bottom and the sidewall, respectively.

4. Conclusions

Downstream of the sluice gate or weir, wave-type flows may occur under no tailwater conditions in a stilling basin. Experimental tests were conducted on five different sill configurations, including the sill position and the sill height. Five test unit discharges between 0.154 m^2/s and 0.230 m^2/s were conducted. The main findings are summarized as follows:

(1) When a sill is located near the upstream weir flow (i.e., the weir toe in this study), the jump types of the wave flow can be classified as submerged and non-submerged. The submerged wave type flow corresponding to a higher relative sill height was relevant for obtaining a better aeration effect.

(2) The ambient pressure head of the wave-type flow (i.e., the bottom pressure of the stilling basin) is strongly influenced by the flow pattern. Pressure fluctuations were more significant in the vicinity of the sill, and these are caused by the movement of the turbulent region of the jump, especially for the change in wave-type flow from a submerged jump to a non-submerged jump. The streamwise mean bottom pressure

profile revealed the existence of three distinct flow zones: (1) deflection zone, (2) jump zone, and (3) wave impact zone. There were two peak pressure points along the stilling basin, and these values can be distinguished by the upstream Froude number and the position and height of the sill.

(3) The air concentrations on the bottom and the sidewall were also affected by the flow pattern. For a given sill-controlled stilling basin, the air concentrations on the bottom and the sidewall decreased with increasing unit discharges. The flow zone within the vicinity of the sill had slight air entrainment and significant pressure fluctuations, which may be prone to cavitation. Thus, this region near the sill should be focused upon in order to provide protection.

The findings from this study have the potential to expand the application of sill-controlled stilling basins in hydraulic engineering by establishing new relationships. Additionally, the results can be used to improve the accuracy of CFD models in predicting wave-type flow behavior.

Author Contributions: Conceptualization, Y.Z.; methodology, Y.Z.; validation, H.Z.; formal analysis, J.H.; investigation, F.B.; resources, Y.Z.; data curation, Y.Z.; writing—original draft preparation, Y.Z.; writing—review and editing, H.Z. and Y.Z.; visualization, J.H.; funding acquisition, Y.Z. and J.W. All authors have read and agreed to the published version of the manuscript.

Funding: This research is supported by the Chinese Scholarship Council (CSC), National Natural Science Foundation of China (Grant No. 51809079), the Scientific and Technological Program of Zhejiang Water Resources Department (RB2119, and RC2143), the Joint Funds of the Zhejiang Provincial Natural Science Foundation of China (Grant No. LZJWY23E090002), the Nanxun Young Scholar, and the Research Center for Digital Economy and Sustainable Development of Water Resources, Zhejiang University of Water Resources and Electric Power (xrj2022012).

Institutional Review Board Statement: Not applicable.

Informed Consent Statement: Not applicable.

Data Availability Statement: All data, models, and code generated or used during the study are available from the corresponding author by request.

Conflicts of Interest: The authors declare no conflict of interest.

Notations

The following symbols are used in this paper:

P	weir height (m)
l_s	length of the stilling basin from the weir toe (m)
s	sill height (m)
h_s	positive step height (m)
Q	inflow discharge (m^3/s)
q_w	inflow unit discharge (m^2/s)
y_0	upstream flow depth (m)
y_1, y_2	supercritical flow depth upstream and downstream of the sill (m)
y_4	flow depth at the terminal section of the weir (m)
v_1, v_2	supercritical flow velocity upstream and downstream of the sill (m/s)
H_p	pressure head (m)
C_b, C_s	air concentrations on the bottom and the sidewall
F_1	upstream Froude number
F_2	downstream Froude number

References

1. Carvalho, R.F.; Lemos, C.M.; Ramos, C.M. Numerical computation of the flow in hydraulic jump stilling basins. *J. Hydraul. Eng.* **2008**, *46*, 739–752. [CrossRef]
2. Manoochehr, F.M.; Sadegh, H.; Babak, L.A.; Peyman, A. Reduction of stilling basin length with tall end sill. *J. Hydrodyn.* **2011**, *23*, 498–502. [CrossRef]

3. Tajabadi, F.; Jabbari, E.; Sarkardeh, H. Effect of the end sill angle on the hydrodynamic parameters of a stilling basin. *Eur. Phys. J. Plus.* **2018**, *133*, 10. [CrossRef]
4. Zhou, Y.; Wu, J.H.; Qian, S.T.; Ding, C.M.; Pan, G.Y. Discussion of "Types I, II, III, and IV Stilling Basin Performance for Stepped Chutes Applied to Embankment Dams" by Sherry L. Hunt and Kem C. Kadavy. *J. Hydraul. Eng.* **2023**, *149*, 07022008. [CrossRef]
5. Hager, W.H.; Li, D. Sill-controlled energy dissipator. *J. Hydraul. Res.* **1992**, *30*, 165–181. [CrossRef]
6. Kang, J.G.; Yeo, H.K.; Lee, K.C.; Choi, N.J. Experimental study on flow characteristic and wave type flow at downstream of stepped weir. *J. Korea Water Resour. Assoc.* **2010**, *43*, 41–49. [CrossRef]
7. Ohtsu, I.; Yasuda, Y.; Hashiba, H. Incipient jump conditions for flows over a vertical sill. *J. Hydraul. Eng.* **1996**, *122*, 465–469. [CrossRef]
8. Eldesoky, I.M.; Abdelsalam, S.I.; Abumandour, R.M.; Kamel, M.H.; Vafai, K. Interaction between compressibility and particulate suspension on peristaltically driven flow in planar channel. *Appl. Math. Mech.* **2017**, *38*, 137–154. [CrossRef]
9. Mossa, M.; Petrillo, A.; Chanson, H. Tailwater level effects on flow conditions at an abrupt drop. *J. Hydraul. Res.* **2003**, *41*, 39–51. [CrossRef]
10. Ferreri, G.B.; Nasello, C. Hydraulic jumps at drop and abrupt enlargement in rectangular channel. *J. Hydraul. Res.* **2002**, *40*, 491–505. [CrossRef]
11. Kawagoshi, N.; Hager, W. Wave type flow at abrupt drops: I. Flow geometry. *J. Hydraul. Res.* **1990**, *28*, 235–252. [CrossRef]
12. Eroğlu, N.; Tokyay, N. Statistical approach to geometric properties of wave-type flow occurring at an abrupt drop. *J. Fac. Eng. Archit. Gazi Univ.* **2012**, *27*, 911–919.
13. Eroğlu, N.; Taştan, K. Local Energy Losses for Wave-Type Flows at Abrupt Bottom Changes. *J. Irrig. Drain. Eng.* **2020**, *146*, 04020029. [CrossRef]
14. Huang, G.; Diao, M.; Jiang, L.; Wang, C.A.; Jia, W. Experimental Study on Wave Characteristics of Stilling Basin with a Negative Step. *Entropy* **2022**, *24*, 445. [CrossRef]
15. Zhou, Y.; Wu, J.H.; Qian, S.T.; Ma, F.; Hu, J.Y. Discussion of "Local Energy Losses for Wave-Type Flows at Abrupt Bottom Changes" by Nihat Eroglu and Kerem Tastan. *J. Irrig. Drain. Eng.* **2021**, *147*, 07021007. [CrossRef]
16. Padulano, R.; Fecarotta, O.; Del Giudice, G.; Carravetta, A. Hydraulic design of a USBR Type II stilling basin. *J. Irrig. Drain. Eng.* **2017**, *143*, 04017001. [CrossRef]
17. Zhou, Y.; Wu, J.H.; Ma, F.; Qian, S.T. Experimental investigation of the hydraulic performance of a hydraulic-jump-stepped spillway. *KSCE J. Civ. Eng.* **2021**, *25*, 3758–3765. [CrossRef]
18. Hager, W.H.; Bremen, R. Classical hydraulic jump: Sequent depths. *J. Hydraul. Res.* **1989**, *27*, 565–585. [CrossRef]
19. Hager, W.H.; Bretz, N.V. Hydraulic jumps at positive and negative steps. *J. Hydraul. Res.* **1986**, *24*, 237–253. [CrossRef]
20. Hunt, S.L.; Kadavy, K.C. Types I, II, III, and IV stilling basin performance for stepped chutes applied to embankment dams. *J. Hydraul. Eng.* **2021**, *147*, 06021004. [CrossRef]
21. Stojnic, I.; Pfister, M.; Matos, J.; Schleiss, A.J. Effect of 30-degree sloping smooth and stepped chute approach flow on the performance of a classical stilling basin. *J. Hydraul. Eng.* **2021**, *147*, 04020097. [CrossRef]
22. Hager, W.H.; Sinniger, R. Flow characteristics of the hydraulic jump in a stilling basin with an abrupt bottom rise. *J. Hydraul. Res.* **1985**, *23*, 101–113. [CrossRef]
23. Sobani, A. Pressure fluctuations on the slabs of stilling basins under hydraulic jump. In Proceedings of the 11th International Conference on Hydroinformatics, New York, NY, USA, 17–21 August 2014.
24. Peterka, A.J. The effect of entrained air on cavitation pitting. In Proceedings of the Proceedings: Minnesota International Hydraulic Convention, Minneapolis, MN, USA, 1–4 September 1953; pp. 507–518.